

Atmospheric pressure X-ray photoelectron spectroscopy apparatus: Bridging the pressure gap

J. J. Velasco-Vélez, V. Pfeifer, M. Hävecker, R. Wang, A. Centeno, A. Zurutuza, G. Algara-Siller, E. Stotz, K. Skorupska, D. Teschner, P. Kube, P. Braeuninger-Weimer, S. Hofmann, R. Schlögl, and A. Knop-Gericke

Citation: [Review of Scientific Instruments](#) **87**, 053121 (2016); doi: 10.1063/1.4951724

View online: <http://dx.doi.org/10.1063/1.4951724>

View Table of Contents: <http://scitation.aip.org/content/aip/journal/rsi/87/5?ver=pdfcov>

Published by the [AIP Publishing](#)

Articles you may be interested in

[New developments in high pressure x-ray spectroscopy beamline at High Pressure Collaborative Access Team](#)

Rev. Sci. Instrum. **86**, 072206 (2015); 10.1063/1.4926888

[Closing the pressure gap in x-ray photoelectron spectroscopy by membrane hydrogenation](#)

Rev. Sci. Instrum. **86**, 053104 (2015); 10.1063/1.4921353

[Sub-nanosecond time-resolved ambient-pressure X-ray photoelectron spectroscopy setup for pulsed and constant wave X-ray light sources](#)

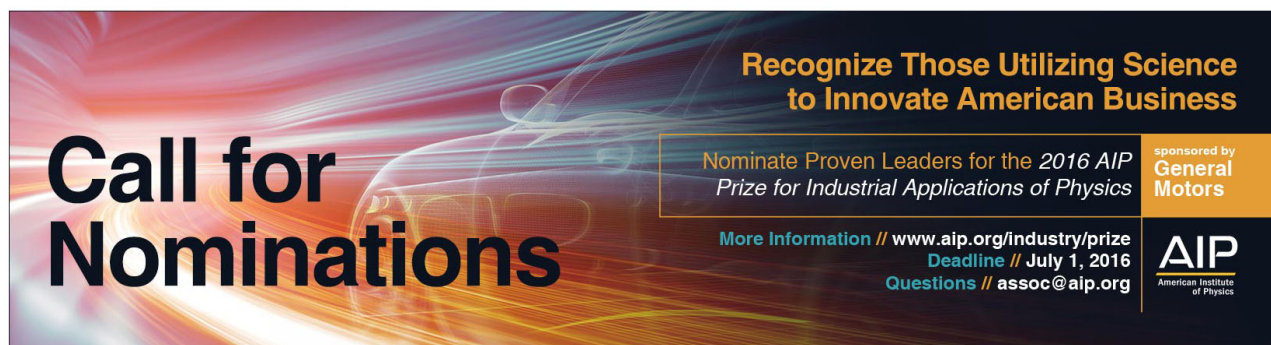
Rev. Sci. Instrum. **85**, 093102 (2014); 10.1063/1.4894208

[A compact, sample-in-atmospheric-pressure soft x-ray microscope developed at Pohang Light Source](#)

Rev. Sci. Instrum. **81**, 063702 (2010); 10.1063/1.3432000

[Note: A combined aerodynamic lens/ambient pressure x-ray photoelectron spectroscopy experiment for the on-stream investigation of aerosol surfaces](#)

Rev. Sci. Instrum. **81**, 016106 (2010); 10.1063/1.3276714



Call for Nominations

Recognize Those Utilizing Science to Innovate American Business

Nominate Proven Leaders for the *2016 AIP Prize for Industrial Applications of Physics*

More Information // www.aip.org/industry/prize
Deadline // July 1, 2016
Questions // assoc@aip.org

sponsored by
General Motors

AIP
American Institute of Physics

Atmospheric pressure X-ray photoelectron spectroscopy apparatus: Bridging the pressure gap

J. J. Velasco-Vélez,^{1,2,a)} V. Pfeifer,² M. Hävecker,^{1,a)} R. Wang,³ A. Centeno,⁴ A. Zurutuza,⁴ G. Algara-Siller,² E. Stotz,² K. Skorupska,¹ D. Teschner,² P. Kube,² P. Braeuninger-Weimer,³ S. Hofmann,³ R. Schlögl,^{1,2} and A. Knop-Gericke²

¹*Department of Heterogeneous Reactions, Max Planck Institute for Chemical Energy Conversion, Mülheim an der Ruhr 45470, Germany*

²*Department of Inorganic Chemistry, Fritz-Haber-Institut der Max-Planck-Gesellschaft, Berlin 14195, Germany*

³*Engineering Department, University of Cambridge, Cambridge CB3 0FA, United Kingdom*

⁴*Graphenea, San Sebastian 20018, Spain*

(Received 1 February 2016; accepted 9 May 2016; published online 25 May 2016)

One of the main goals in catalysis is the characterization of solid/gas interfaces in a reaction environment. The electronic structure and chemical composition of surfaces become heavily influenced by the surrounding environment. However, the lack of surface sensitive techniques that are able to monitor these modifications under high pressure conditions hinders the understanding of such processes. This limitation is known throughout the community as the “pressure gap.” We have developed a novel experimental setup that provides chemical information on a molecular level under atmospheric pressure and in presence of reactive gases and at elevated temperatures. This approach is based on separating the vacuum environment from the high-pressure environment by a silicon nitride grid—that contains an array of micrometer-sized holes—coated with a bilayer of graphene. Using this configuration, we have investigated the local electronic structure of catalysts by means of photoelectron spectroscopy and in presence of gases at 1 atm. The reaction products were monitored online by mass spectrometry and gas chromatography. The successful operation of this setup was demonstrated with three different examples: the oxidation/reduction reaction of iridium (noble metal) and copper (transition metal) nanoparticles and with the hydrogenation of propyne on Pd black catalyst (powder). *Published by AIP Publishing.* [<http://dx.doi.org/10.1063/1.4951724>]

I. INTRODUCTION

Catalysis is a term introduced by Berzelius in 1835 describing the property of some substances to increase the rate of reactions without being consumed themselves.¹ The most important catalytic effect is the increase of reaction rate by means of lowering the activation energy. Although the equilibrium between reactants and products is determined only by thermodynamics, catalysts allow equilibrium to be established quicker. Therefore, heterogeneous catalysis is extensively used in industrial processes to reduce operating temperatures and lower production costs.² Furthermore, catalysis represents the principal operation concept in different devices such as solid state sensors,³ chemical separators,⁴ solid oxide fuels cells⁵ and is used in biological applications.⁶ Another important application area of catalysts is the treatment of greenhouse gases (GGs) and the mitigation of their effects.⁷ The ultimate objective in catalysis research is to reach the ideal geometry and electronic properties of catalysts for a desired reaction. However, the analysis of the electronic surface structure under real operating conditions is one of the main challenges in heterogeneous catalysis.

X-ray based spectroscopy techniques provide fundamental information about the electronic structure of catalyst materials. However, since all of the X-ray-based methods that yield insight into the electronic structure of catalysts—in particular photoelectron spectroscopy (PES) as well as soft X-ray emission (XES) and X-ray absorption (XAS) spectroscopies in the soft range—require vacuum conditions, they are hardly compatible with gases at atmospheric pressures. The discrepancy between higher operating pressures applied in catalytic processes and lower measurement pressures accessible during surface characterization is known in the community as the “pressure gap.”⁸ To bridge this gap, new experimental and instrumental methods have been developed such as Ambient Pressure XPS (AP-XPS), which allows the collection of photoelectrons at pressures in the millibar range.⁹ The wealth of information provided by these experimental setups is of prime importance to the understanding of complex systems. However, the study of solid-gas interfaces with partial pressures beyond a few tens of millibars remains a major challenge. Recently, this technique was extended to higher kinetic energy (HAXPES). Notably, this approach combined with a small aperture nozzle increases the operation pressure up to 100 mbars.^{10,11} The higher kinetic energies (KEs) reduce the scattering of photoelectrons in the gas phase and increase the inelastic mean free path in the solid, which allows deeper material profile analysis. In addition, the inclusion of a shaped

^{a)}Authors to whom correspondence should be addressed. Electronic addresses: velasco@fhi-berlin.mpg.de and mh@fhi-berlin.mpg.de

mesh lens allows the collection of high energy photons at higher pressures.¹¹

The pressure reached by HAXPES can be overcome by using photon-in/photon-out (PIPO) techniques in the soft X-ray range with an information depth of a few hundred nanometers.¹² The penetration depth of X-rays in PIPO techniques permits separation of the 1 bar gas phase from the UHV chamber containing soft X-ray source and detector via a thin silicon nitride membrane and thus the study of the material of interest at atmospheric pressure. In fluorescence yield (FY), PIPO techniques provide bulk information due to the fact that the photons are less attenuated than electrons while in photon in/electron techniques like total electron yield (TEY) provide surface/sub-surface information due to the fact that the photons are less attenuated than electrons.¹³ Nonetheless, a complete understanding of chemical reactions requires the characterization of the chemical composition at the outermost interface. Additionally, the evaluation of a depth profile of species perpendicular to the surface is highly desirable. Such depth resolution enables the discrimination between species located close to the interface or in the bulk, which is not possible with PIPO techniques. This problem can be resolved by using photoelectron spectroscopy where the penetration depth can be tuned by changing the energy of the incoming photons creating photoelectrons of different kinetic energy and hence different degree of inelastic scattering in the solid. The photoelectron signal yields information about the interface

structure with nanometer sensitivity as well as local potential energy variations. Hence, XPS can describe the surface composition, oxidation state, and electronic structure in a depth resolved manner.¹⁴ Here we introduce an atmospheric pressure X-ray photoelectron spectroscopy gas cell based on an array of micro holes coated with graphene that solves the mechanical stability problem of free standing graphene covering large open areas and still provides high transmission for low kinetic energy electrons (higher than 400 eV) combined with a high rate of fabrication reproducibility. The newly developed gas cell follows the concept introduced by Velasco-Vélez *et al.*¹⁵ for an electrochemical *in situ* flow liquid cell.

II. TECHNICAL APPROACH

In presence of gases, inelastic scattering with gas molecules prevents the photoelectrons that are generated by incoming X-rays from being collected effectively. Figure 1(a) shows the AP-XPS end-station located at the Innovative Station for In Situ Spectroscopy (ISSS)¹⁶ beamline (BESSY II, Berlin). A photoelectron transparent membrane (graphene) was implemented in the gas cell to separate the atmospheric pressure inside the cell from the vacuum on the outside and to maintain UHV conditions in the analyzer (as shown in Figure 1(d2)). Using this approach, a reaction gas cell was developed, allowing controlled dosing of reaction gases in

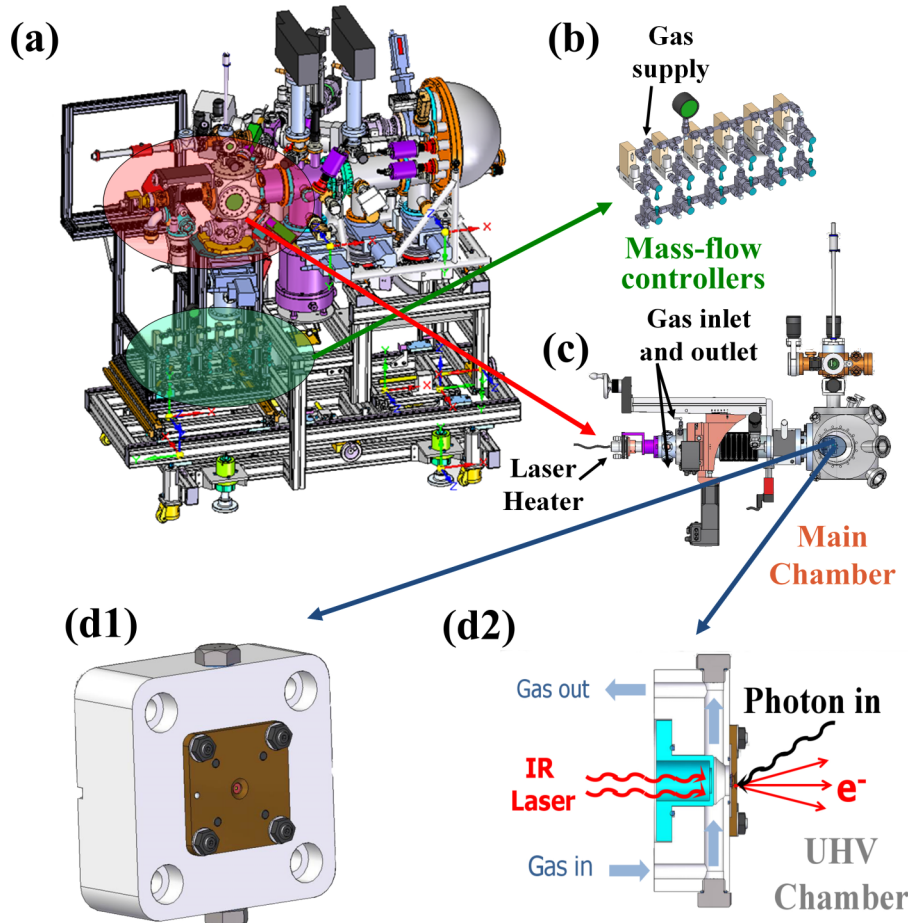


FIG. 1. (a) AP-XPS setup. (b) Mass flow controllers. (c) Main-chamber including the manipulator. (d1) Gas cell inlay including (d2) its cross section.

a flow through scheme at 1 bar total pressure. Figure 1(c) shows the main-chamber, including the manipulator. The whole reaction cell is mounted in a precision-motion stage (manipulator) that can accurately be adjusted in the x, y, and z directions relative to the beam and analyzer entrance aperture (“nozzle”). In such a way, the sample can be adjusted to an optimal position. The base of the gas cell provides feedthroughs for electrical contacts used to ground or bias the samples and connect the thermocouples. Measuring the sample drain current also becomes feasible. In this section, the technical characteristics of this setup are described in detail.

A. Gas cell: Flow controller, heater and temperature monitoring, gas analysis

The gas feed into the cell is achieved via a stainless-steel tube inlet (see Figure 1(c)) and is regulated by Bronkhorst mass flow controllers (see Figure 1(b)). Basic estimation of the gas flows in the inlet and outlet gas cell lines suggests that there should not be a noticeable pressure drop between the pressure in the cell, the sample container, and the outgoing tubing. Helium is fed into the cell via a mass flow controller as an inert balance gas, which allows the system to operate at atmospheric pressures with relative low partial pressures of other fed gases.

Figure 1(c) shows the main-chamber, including the manipulator and the laser heater. Heating of the sample can be provided by various means. Either by direct heating of the sample deposited on the membrane (e.g., by an IR laser) or by indirect methods like heating the incoming gas. Here, we describe an indirect laser heating that avoids large temperature gradients on the sample but still acts locally on the sample material. Heating of the sample is provided by an infrared laser ($p_{\max} = 60$ W, 808 nm) equipped with an optical system that forms a uniform heating field of 5×5 mm² at the rear of the target. Using this approach, a stainless-steel plate is heated with the IR source which heats the gas and therefore the sample is heated indirectly. The laser is located outside the manipulator and the leak-tightness and IR transmission is assured by a special viewport flange. This IR laser heating system has proven its reliable performance in several *in situ* electron spectroscopy setups developed in our group.¹⁷ A

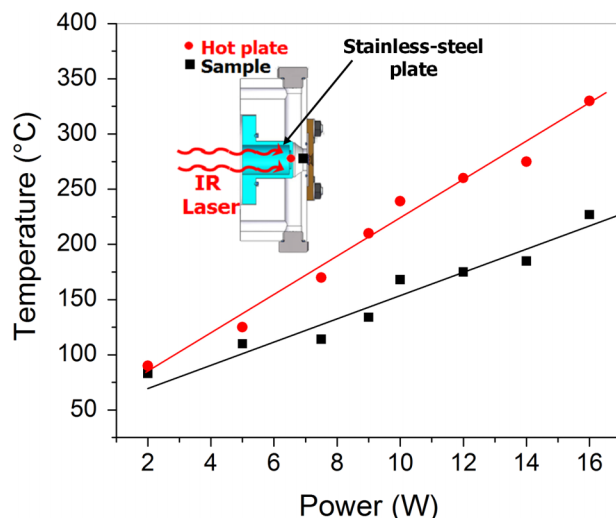


FIG. 2. Temperatures in the hot plate and in the sample versus laser power.

stainless-steel plate is heated by the IR laser and a small part of cell volume is heated by radiation and gas convection (see Figure 1(d)). Temperature control can be achieved via two thermocouples placed in the vicinity of the sample surface and in the stainless-steel heating plate, respectively. The trends in the temperature in the hot-plate and in the sample depend on the laser optical power and are indicated in Figure 2. Heating with a laser avoids the problems associated with thermo-resistors in which the resistive current forms stray magnetic fields.

The outlet gas line is connected directly to a fast gas-chromatograph (VARIAN μ -GC CP4900 equipped with 4 independent detection channels), allowing the identification and quantification of chemical products of the catalytic reaction. In addition, a fraction of the outgoing gas stream is fed into an electron impact mass spectrometer to analyze its composition.

B. Graphene membrane

Figure 3(a) shows a sketch of the hole array grid coated with graphene, and a scanning electron microscopy (SEM) image of the holes array

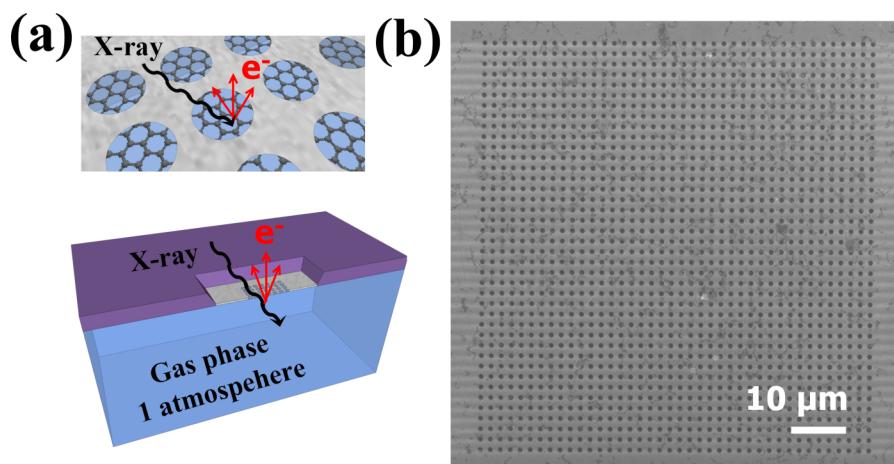


FIG. 3. (a) Membrane sketch. (b) SEM image of the holes array ($80 \mu\text{m} \times 80 \mu\text{m}$ array with one $1 \mu\text{m}$ diameter holes) fully coated by a bi-layer graphene (BLG).

image of this grid coated graphene is shown in Figure 3(b). The chemical-vapour deposited (CVD) graphene was grown on Cu foil and transferred to the Si_3N_4 grids in the procedure described by Velasco-Vélez *et al.*¹⁵ Using the gas-flow cell described in Figure 1(d), a pressure of $\sim 10^{-6}$ mbar arose in the main chamber during flowing gas at 1 atm on the other side of the membrane. The pressure in the main-chamber is the same for a reference solid silicon wafer sample (200 μm thick), suggesting excellent sealing properties of the graphene layer. Furthermore, Figure S1 of the supplementary material¹⁸ shows the lack of a peak related to the gas-phase collected at 350 eV KE during dosing N_2 (red curve), which is a good indication of the leak tightness of these membranes. Since electron transmission of bi-layer graphene (BLG) is pretty reduced for very low E_{kin} .¹⁹ In addition to traditional XAS operation in fluorescence yield (FY) mode, this approach also allows the detection of photo and Auger electrons generated near the solid/gas interface.

III. EXPERIMENTAL CASES

The performance of this setup was evaluated by model reactions with three different classes of materials: the oxidation-reduction of transition metal (Cu) and noble metal (Ir) nanoparticles and the selective hydrogenation of alkynes into alkanes/alkenes on a powder catalyst (solid Pd black, from ALDRICH with a surface area 40-60 m^2/g , 99.95% trace metal basis). These experiments were performed using the ISSS beamline of BESSY II (Berlin, Germany) as a tunable soft X-ray source.

A. Oxidation of noble metals: Ir

Iridium nanoparticles of 2-5 nm size were sputter-deposited on bilayer graphene as the TEM image shows (see Figure 4(b)). Figure S2 indicates that KEs higher than 400 eV are required to generate photoelectrons with enough energy

to pass through the BLG.¹⁸ Thus, the presence of iridium on the side of graphene exposed to the HV (analyzer) was ruled out by collecting the Ir 4f spectra at different KEs. The membrane was mounted in the gas cell and different gas mixtures were flowed at a temperature of 215 °C at 1 bar total pressure. First, a mixture of 5% H_2 in He (balance gas) was flowed and later a mixture of 20% O_2 in He was introduced to the cell. The electronic structure of iridium was probed by the Ir 4f line shape by *in situ* measurement of photoelectrons with 600 eV kinetic energy by a hemispherical electron energy analyzer (see Figure 4(c)). XP Ir 4f_{7/2} and Ir 4f_{5/2} spectra of metallic iridium show two sharp asymmetric peaks centered at 60.9 eV and 63.9 eV, respectively, while rutile-type IrO_2 displays peaks at 61.7 eV and 64.7 eV.²⁰ Broad peak profiles indicate the presence of multiple iridium species. Figure 4(c) shows a superposition of the normalized Ir 4f spectra under the two gas flows described at 1 atmosphere. A broader Ir 4f peak evolves in the presence of oxygen at ~ 215 °C, which is related to the formation of iridium oxide species. Otherwise, the iridium is reduced in presence of H_2 , as the sharper peak indicates. The difference between the Ir 4f spectra under oxidizing and reducing atmospheres is shown in Figure 4(c) (gray curve). The difference spectrum highlights the decay in the metallic iridium contribution (peaks at 60.9 eV and 63.9 eV) and the increase in the oxidized species (61.7 eV and 64.7 eV) in the oxidizing atmosphere. Consequently, these measurements show that the oxidation state of the sputtered Ir nanoparticles on bilayer graphene can be followed by photoelectron spectroscopy at 1 bar total gas pressure, which is a noteworthy pressure for this spectroscopic technique.

B. Oxidation of transition metals: Cu

The oxidation state of sputter-deposited copper nanoparticles (2-5 nm) was probed by XPS and near edge X-ray absorption fine structure (NEXAFS or XAS for short) at room

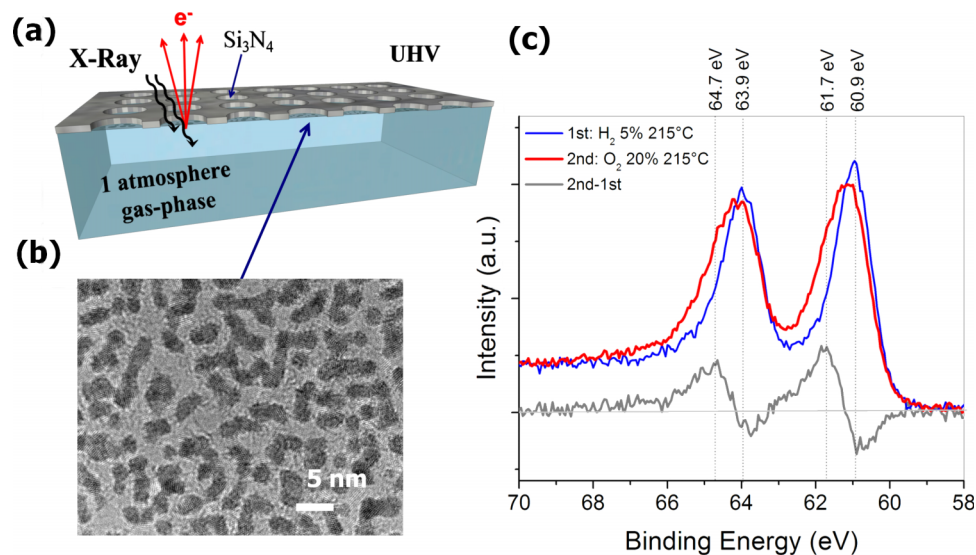


FIG. 4. (a) Schematic of the operation mode including (b) TEM measurement of the sputtered nanoparticles on BLG (2-5 nm) and (c) the Ir 4f XP spectra under several gases exposures ($P = 1$ bar, $T = 25$ °C).

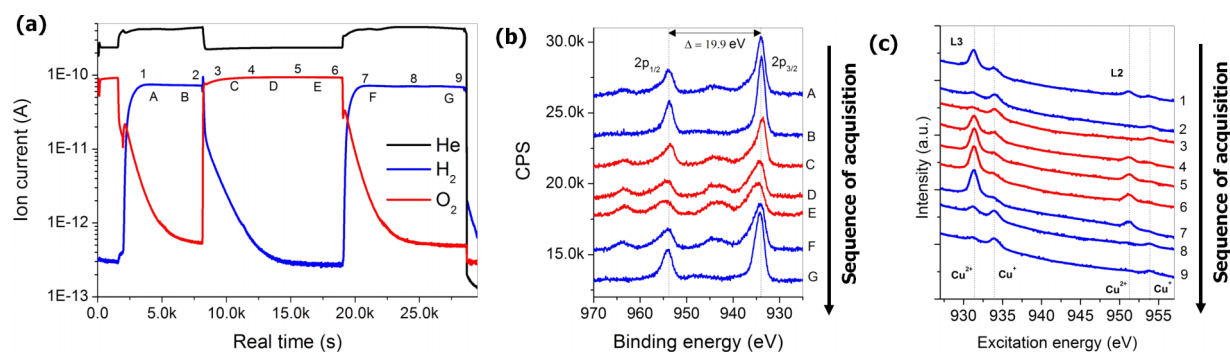


FIG. 5. (a) Mass spectra collected under different gas exposure. (b) Cu 2p XP and (c) Cu L_{3,2}-edges XA spectra under different gas exposure ($P=1$ bar, $T=25$ °C).

temperature and 1 bar total pressure. XPS was performed using the hemispherical spectrometer located at the ISSS beamline. The Cu L-edge was collected in total electron yield (TEY-XAS) by the current collected by a Faraday cup located outside of the gas cell in the main chamber (UHV). Using this approach, the oxidation state of the Cu nanoparticles in the presence of oxidizing or reducing gases was identified. The gas mixture was monitored online by mass spectroscopy. Figure 5(a) shows the mass profile of the gas sequence flowed inside the gas cell. We started with a reducing atmosphere of 5% H₂ in He. The sequence of exposure continues with an oxidizing atmosphere of 20% O₂ and ends with a reducing atmosphere of 5% H₂ in He. The oxidation state of Cu was determined from the Cu 2p_{3/2} and Cu 2p_{1/2} XP spectra (collected at 600 eV KE), which show a broader peak in an oxidizing atmosphere than in a reducing feed (see Figure 5(b)). Otherwise, XAS probes the unoccupied orbitals and is sensitive to the chemical state of copper. The L_{3,2}-edges provide unequivocal information about the oxidation state of the copper nanoparticles by characteristic Cu²⁺ and Cu⁺ peaks at ~931 eV and ~934 eV,²¹ respectively. Accordingly, Figure 5(c) shows the reduction of the copper nanoparticles from a Cu²⁺ to a Cu⁺ state in presence of H₂ at 1 bar total pressure. Switching the gases from H₂ to O₂, the copper nanoparticles show a slow oxidation from Cu⁺ to Cu²⁺ due to the low temperature oxidation/reduction process. Finally, changing the gas back to H₂ prompts the re-reduction of the copper nanoparticles. The changes determined as a function of the transition times for processes occurring in the oxygen and hydrogen regions have been plotted in Figure 5. Hysteresis effects can originate from several sources. Kinetically, if the rate of desorption process differs from that of the adsorption process or if the sorbate/sorbent system forms metastable domains, the system undergoes an irreversible phase transition to a more stable form than before, which can yield a kinetic reaction explanation. Nevertheless, Figure S3 shows the presence of Cu impurities on the graphene due to the transfer process in the surface exposed to the HV (analyzer) as the Cu 2p spectrum collected at 200 eV KE proves (these impurities were found in 100% of the membranes analyzed).¹⁸ It implies that the KE energy of the photoelectrons should be high enough to assure that most of the signal is coming from the Cu located underneath the graphene. As we mentioned above, the measurements were performed at 600 eV KE for

the Cu 2p spectra assuring the signal is from the copper located in the side exposed to the gas.

C. The hydrogenation of alkynes on Pd black catalyst

Palladium is one of the most important hydrogenation catalysts and is industrially relevant in the selective hydrogenation of alkynes into alkenes and alkanes. A carbon-carbon triple bond can be hydrogenated partially to the alkene or fully to the alkane groups. Photoelectron spectroscopy was applied to investigate changes in the chemical nature of the active species and in particular to elucidate the electronic structure of the catalyst under reaction conditions. Online gas chromatography has been used to relate the electronic structure with the catalytic performance. Using the setup described above, we explored the hydrogenation of propyne to propene and propane on a coarse sponge like form of palladium, which has a large surface area, referred to as palladium black catalyst. Figure 6 shows the Pd 3d_{5/2} spectra and the gas chromatogram collected at room temperature and 1 atmosphere pressure under three different flows of gases: (a) 1 atm of He, (b) 1 atm 41.2% H₂ in He, (c) 1 atm H₂/C₃H₄ (39.8%/3.3%) feed gases in He. The catalytic activity of the drop casted Pd black powder (red curve in the GC spectra) was confirmed by comparison with an inactive SiO_x wafer (black curve in the GC trace), as shown in Figure 6(c). Photoelectron spectroscopy was applied to investigate changes in the chemical nature of the active species, and in particular, to elucidate the electronic structure of the catalyst under reaction conditions. Commercial Pd black powder was deposited on the graphene membrane by drop casting from Pd nanoparticles suspended in acetone. Figure S4 shows the absence of Pd-black particles on the part exposed to the HV (analyzer) was ruled out by the Pd 3d spectra collected at different KEs.¹⁸ After that the membrane was mounted in the gas cell and tested under reaction conditions. First of all, the cell was purged with a continuous flow of He and the Pd 3d_{5/2} spectra were collected (Figure 6(a)). The Pd black in the “as delivered” state in He (1 atm) shows two peaks in the Pd 3d_{5/2} spectrum. The peak at binding energy BE ~ 335.0 eV is ascribed to zero-valent metallic palladium, whereas the peak at BE ~ 336.7 eV is associated to the divalent PdO species. Subsequently 41.2% H₂ in He was flowed in the cell. The H₂ was detected at the outlet of the gas line as the GC shows in the mole sieve MS5 column (Figure 6(b))

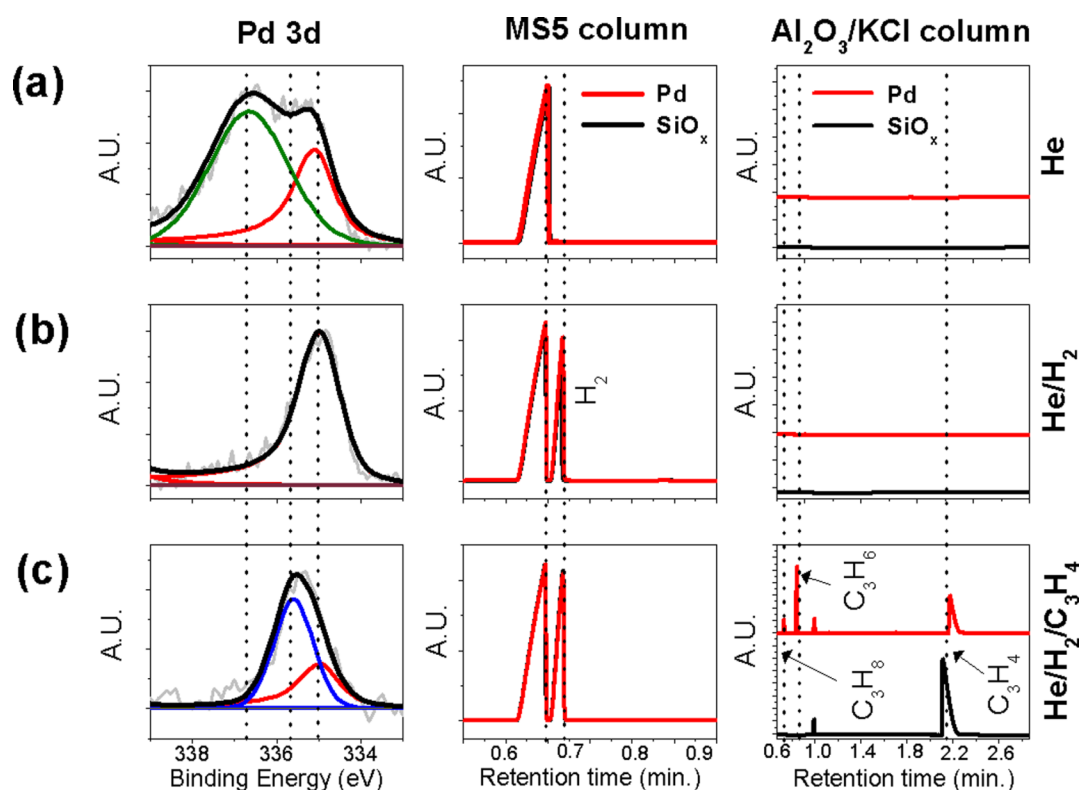


FIG. 6. (a) Pd 3d XP spectra and gas chromatography traces (VARIAN μ GC 4900) using a mol sieve MS5 column (VARIAN CP740148) and $\text{Al}_2\text{O}_3/\text{KCl}$ column (AGILENT 494001440): (a) He, (b) He/H_2 , and (c) $\text{He}/\text{H}_2/\text{C}_3\text{H}_4$ gas mixtures.

(VARIAN μ GC 4900). Under such conditions, the peak at 335.0 eV prevails and the line at 336.7 eV vanished, which indicated that the Pd catalyst was reduced.²² Finally, the gas was switched to a flow mixture of $\text{H}_2/\text{C}_3\text{H}_4$ (39.8%/3.3%) in He. The $\text{Al}_2\text{O}_3/\text{KCl}$ column detects hydrocarbons, and the peak with the highest retention time corresponds to the educt propyne while the first two peaks can be assigned to propane and propene, respectively. (The third peak is a butene impurity in the propyne feed.) The comparison clearly suggests that Pd black produced mainly propene and propane in smaller quantities, whereas no reactivity can be ascribed to the dummy sample. Under these conditions, Pd 3d $5/2$ spectra undergo to a shift to higher BE (~ 335.6 eV) associated with carbon incorporation into Pd (PdC $_x$ formation), which is the active phase of selective alkyne hydrogenation over Pd.²³

IV. CONCLUSIONS

A spectroscopic tool to promote knowledge-based catalyst design has been developed, built, and put into operation. The system allows the investigation of the electronic structure of complex solid-gas interfaces by means of XPS at 1 bar total pressure for the first time. Higher gas pressures might become feasible in the future. Additionally, surface sensitive NEXAFS measurements in the electron yield mode are feasible with the very same cell without any modification. This design overcomes the limit of AP-XPS by allowing the analysis of the electronic structure of complex systems under real atmospheric pressure without the need for a special (i.e., differentially pumped) electron spectrometer

since the pressure during operation of the gas cell in the vacuum tank remains around 10^{-6} mbar. Therefore, this cell design opens up the possibility of reaction studies at higher pressure overcoming the so-called “pressure gap,” which, among other areas, is of prime importance for catalysis and environmental science. These measurements are possible due to the excellent photoelectron transmission, as well as the outstanding properties of graphene such as leak tightness and photoelectron transparency.

ACKNOWLEDGMENTS

We thank the staff at BESSY II of the HZB for operational support at the ISSS beamline under Proposal No. 14201159. This work was funded from EU project GRAFOL Grant No. 285275. We thank Ministry of Education and Science of the Russian Federation (Agreement No. 14.616.21.0007) and Bundesministerium für Bildung und Forschung (Project No. 05K2014) for financial support in the framework of joint Russian-German research project “SYnchrotron and NEutron STudies for Energy Storage (SYNESTESia).” We thank Dr. Mark Greiner and Dr. Travis Jones for helping during the manuscript preparation.

¹J. J. Berzelius, *Annual Report on Progress in Physics and Chemistry [Årsberättelsen om Framsteg i Fysik och Kemi]* (Royal Swedish Academy of Sciences, Stockholm, Sweden, 1885).

²C. N. Satterfield, *Heterogeneous Catalysis in Industrial Practice*, 2nd ed. (McGraw Hill Book Co., 1991).

³N. Yamazoe, *Sens. Actuators, B* **5**(1), 7–19 (1991).

⁴E. J. Henley, J. D. Seader, and D. K. Roper, *Separation Process Principles* (Wiley, 2011).

- ⁵L. Carrette, K. A. Friedrich, and U. Stimming, *Fuel Cells* **1**(1), 5–39 (2011).
- ⁶C. H. Wong and G. M. Whitesides, *Enzymes in Synthetic Organic Chemistry* (Academic Press, 1994), Vol. 12.
- ⁷R. Schlögl, *Angew. Chem., Int. Ed.* **50**(29), 6424–6426 (2011).
- ⁸P. Stoltze and J. K. Nørskov, *Phys. Rev. Lett.* **55**(22), 2502 (1985).
- ⁹D. F. Ogletree, H. Bluhm, G. Lebedev, C. S. Fadley, Z. Hussain, and M. Salmeron, *Rev. Sci. Instrum.* **73**(11), 3872–3877 (2002).
- ¹⁰S. Kaya, H. Ogasawara, L. A. Näslund, J. O. Forsell, H. S. Casalongue, D. J. Miller, and A. Nilsson, *Catal. Today* **205**, 101–105 (2013).
- ¹¹S. Axnanda, E. J. Crumlin, B. Mao, S. Rani, R. Chang, P. G. Karlsson, M. O. M. Edwards, M. Lundqvist, R. Moberg, P. N. Ross, Z. Hussain, and Z. Liu, *Sci. Rep.* **5**, 9788 (2015).
- ¹²A. Knop-Gericke, M. Hävecker, T. Neisius, and T. Schedel-Niedrig, *Nucl. Instrum. Methods Phys. Res., Sect. A* **406**(2), 311–322 (1998).
- ¹³J. J. Velasco-Velez, C. H. Wu, T. A. Pascal, L. Wan, J. Guo, D. Predergast, and M. Salmeron, *Science* **346**(6211), 831–834 (2014).
- ¹⁴K. Siegbahn, *Electron Spectroscopy for Atoms, Molecules and Condensed Matter* (Uppsala University: Fysiska Institutionen, Sweden, 1981).
- ¹⁵J. J. Velasco-Velez, V. Pfeifer, M. Hävecker, R. S. Weatherup, R. Arrigo, C.-H. Chuang, E. Stotz, G. Weinberg, R. Schlögl, and A. Knop-Gericke, *Angew. Chem., Int. Ed.* **54**(48), 14554–14558 (2015).
- ¹⁶See https://www.helmholtz-berlin.de/pubbin/figama_output?modus=einzel&sprache=en&gid=1607 for technical details of the ISIS beamline.
- ¹⁷C. Heine, M. Hävecker, E. Stotz, F. Rosowski, A. Knop-Gericke, A. Trunschke, M. Eichelbaum, and R. Schlögl, *J. Phys. Chem.* **118**, 20405 (2014).
- ¹⁸See supplementary material at <http://dx.doi.org/10.1063/1.4951724> for the leak test and for the element depth profile obtained at different KEs.
- ¹⁹A. Kolmakov, L. Gregoratti, M. Kiskinova, and S. Günther, *Top. Catal.* **59**, 448–468 (2016).
- ²⁰C. S. Fadley and D. A. Shirley, *J. Res. Natl. Bur. Stand., Sect. A* **74**, 543 (1970).
- ²¹G. Vlaic, J. C. J. Bart, W. Cavigiolo, and S. Mobilo, *Chem. Phys. Lett.* **76**(3), 453–459 (1980).
- ²²K. Noack, H. Zbinden, and R. Schlögl, *Catal. Lett.* **4**(2), 145–155 (1990).
- ²³D. Teschner, J. Borsodi, A. Wootsch, Z. Révay, M. Hävecker, A. Knop-Gericke, S. D. Jackson, and R. Schlögl, *Science* **320**(5872), 86–89 (2008).